scientific reports

Check for updates

OPEN

Asymmetry in centrosome maturation revealed through AIR-1 dynamics in the early *Caenorhabditis elegans* embryo

Shayne M. Plourde[1,2], Natalia Kravtsova[3] & Adriana T. Dawes[2,3]✉

Centrosomes are critical organelles associated with the nucleus, consisting of a pair of centrioles surrounded by a cloud of pericentriolar material. They serve as key nucleation sites for microtubule arrays and are essential for positioning the nucleus prior to cell division, but mechanisms for ensuring proper centrosome positioning are not well understood. Previous research has identified asymmetries in microtubule arrays nucleated by centrosomes prior to cell division, including during the first cell cycle in *Caenorhabditis elegans*, as playing a critical role in centrosome positioning, however the origin of this asymmetry remains unclear. To explore potential sources of centrosome asymmetry, we developed a mathematical model of centrosome maturation, distinct from prior models by not presuming any inherent symmetry or asymmetry. We determined model parameters using in vivo data on the recruitment and recovery of GFP-tagged AIR-1 (Aurora kinase A) in early *C. elegans* embryos, enabling precise parameter estimation. Our results reveal an intrinsic asymmetry in centrosome dynamics that highlights the potential for variability in physical centrosome characteristics. These dynamics produce highly consistent microtubule arrays, independent of specific structural details. These findings offer novel insights into centrosome behavior and positioning during cell division and early embryonic development.

The centrosome, consisting of a pair of centrioles surrounded by a cloud of pericentriolar material (PCM), is the cell's primary microtubule organizing center[1,2]. The centrosome nucleates microtubule arrays within the cytoplasm, which are required for fundamental cellular processes including establishing intracellular polarity, and driving cellular division. Precise regulation of the timing and placement of cellular division is critically important for proper cell fate determination, and defects in centrosome positioning are associated with disease processes including cancer metastasis[3]. Asymmetries in microtubule arrays are thought to play an important role in centrosome positioning[4]; however, it remains unclear whether this microtubule array asymmetry is related to asymmetries within the centrosomes themselves.

Exploiting the high conservation of centrosome-associated factors, the early embryos of the nematode *Caenorhabditis elegans* provide an ideal model for investigating potential centrosome asymmetries[5]. During fertilization in the *C. elegans* zygote, two centrioles are contributed by the sperm along with the paternal pronucleus[6]. These centrioles undergo duplication and maturation, accumulating pericentriolar material (PCM) to form fully functional centrosomes[7]. These developing centrosomes serve as nucleation sites for microtubule (MT) arrays that interact with motor proteins at the cell periphery to position the nucleus prior to cell division[8]. Previous modeling studies have assumed that centrosomes have equal nucleation capabilities, in the absence of conclusive evidence regarding the composition of PCM[9–12]. Current research suggests that the PCM may exist in solid, liquid, or gel-like states (a combination of solid and liquid), highlighting the complexity and potential variability in centrosome structure[5].

In many systems, centrioles possess age-specific markers such as distal appendage proteins, allowing the older (mother) and younger (daughter) centrioles to be segregated to specific cells during division to promote particular cell fates[13,14]; inheritance of the mother centriole is linked to stem cell maintenance in the *Drosophila* germline[15,16] and the developing mouse neocortex[17]. In *C. elegans* embryos, the P-lineage, which gives rise to the germline, undergoes a series of asymmetric divisions, resulting in a larger anterior cell and a smaller posterior germline cell (Fig. 1a). These divisions are critical for development of the worm, as perturbations in the division

[1]Molecular, Cellular, and Developmental Biology Program, The Ohio State University, Columbus, OH, USA. [2]Department of Molecular Genetics, The Ohio State University, Columbus, OH, USA. [3]Department of Mathematics, The Ohio State University, Columbus, OH, USA. ✉email: dawes.33@osu.edu

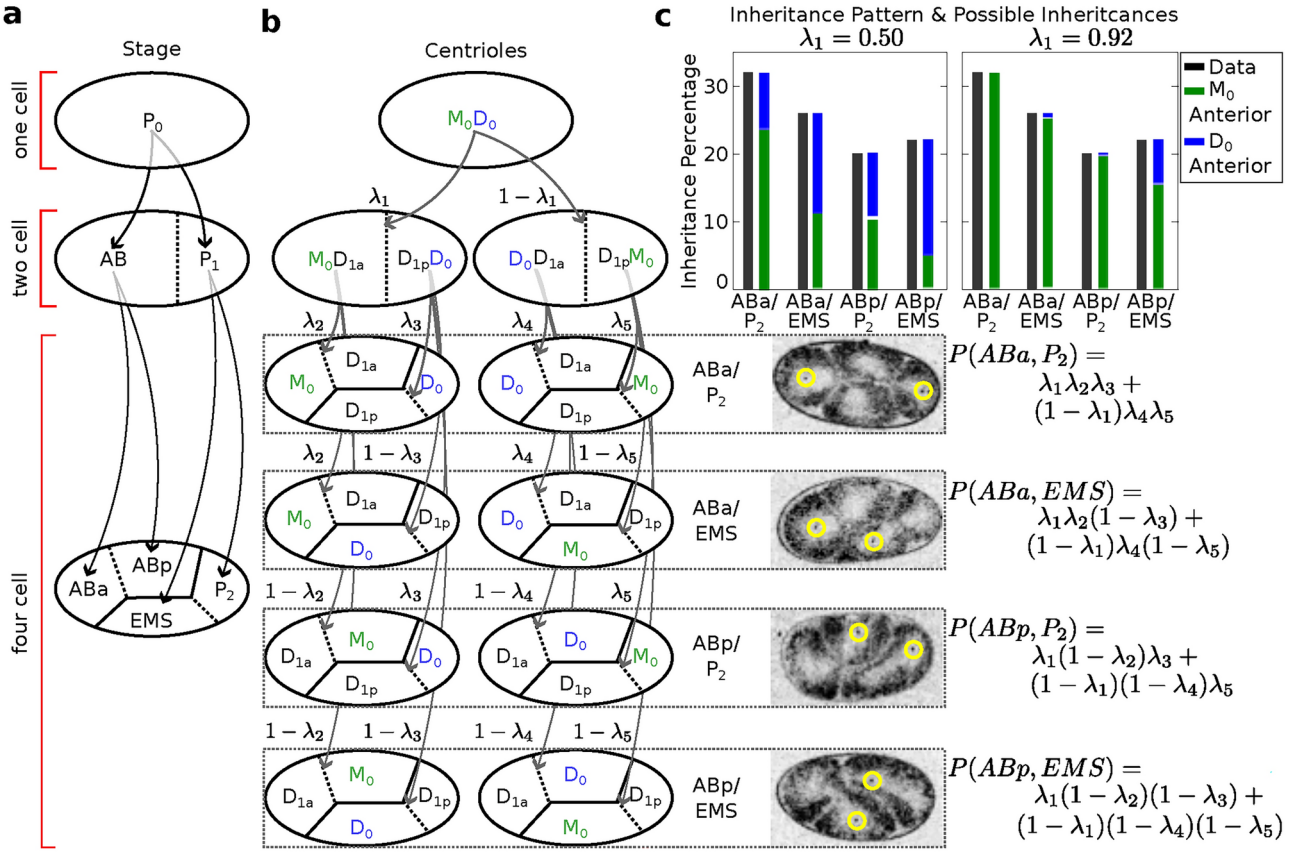

Figure 1. Ambiguous identity of sperm-derived centrioles at the two and four cell stages. (**a**) The divisions leading up to the four-cell stage follow the predetermined pattern shown. (**b**) Schematic of potential inheritance patterns. (**c**) The inheritance pattern percentages for the four possible observable configurations, represented by the black bars, are not significantly different from a uniform distribution. The black bars correspond to experimental data obtained from 65 embryos, each exhibiting two distinct GFP+ centrioles. The colored bars indicate the potential inheritance patterns for the paternal mother centriole (Green) and paternal daughter centriole (Blue), as determined by different choices for λ_1. Example images of the four possible distributions of GFP+ centrioles and their associated probabilities are shown.

plane by as little as 10% can be lethal[18]. However, it remains unclear whether *C. elegans* centrioles possess age related markers, and whether the mother and daughter centrioles are specifically segregated during these early asymmetric divisions.

Previously, our lab demonstrated an asymmetry in the microtubule (MT) arrays nucleated by the two centrosomes in the early *C. elegans* embryo, which play a crucial role in positioning the pronuclear complex before the first division[4]. The lagging centrosome, inherited by the germline cell, forms a smaller and less dense MT array, an asymmetry which our mathematical model indicated as essential for proper centrosome positioning. To investigate a possible unrecognized asymmetry in the associated centrioles and centrosomes, we characterize the inheritance of paternal centrioles through the first two divisions of the *C. elegans* embryo and the recruitment and recovery dynamics of centrosome-associated proteins. Using a novel mathematical model of centrosome maturation calibrated and validated by *in vivo* data, our results reveal potential intrinsic asymmetries in centriole identity and centrosome dynamics, highlighting significant variability in physical centrosome characteristics while still producing similar microtubule arrays. This indicates a high degree of flexibility in centrosome dynamics, enabling consistent and reproducible MT array asymmetry, independent of specific structural details.

Results

Patterns of centriole inheritance

To assess for potential bias in centriole inheritance during the initial divisions of the *C. elegans* embryo, we tracked SAS-4, a stable core protein specific to centrioles. Using GFP-tagged SAS-4 expressed in paternal centrioles, distinguishable up to the 550-cell stage[19], we crossed males with GFP-tagged SAS-4 with feminized hermaphrodites lacking fluorescence. We then monitored paternal centriole inheritance up to the four-cell stage (Fig. 1a). Due to the visual indistinguishability of the mother and daughter sperm-derived centrioles, there are four observable fluorescence patterns among the eight possible configurations (Fig. 1b). Using these patterns, we constructed a probabilistic model (Eq. 10) to determine the probability of centriole inheritance, λ_i, for each

division outcome. Imaging 72 embryos revealed two distinct GFP+ centrioles in 65 cases. The most prevalent inheritance pattern, observed in 21 cases (32.3% of observable patterns), is paternal centriole inheritance to the ABa and P2 cells (Fig. 1c), although the overall distribution is not significantly different from uniform according to the Kolmogorov-Smirnov test, consistent with other reports[20]. A wide range of probability values can produce the same distribution of paternal centriole inheritance, ranging from purely random inheritance of the mother and daughter centrioles ($\lambda_1 = 0.5$) to highly biased and directed inheritance ($\lambda_1 = 0.92$) in the first cell division that still results in the same pattern of fluorescence (Fig. 1c).

Centrosomal AIR-1 recruitment

To determine if the observed asymmetry in microtubule (MT) arrays is associated with centrosome asymmetry, we investigate centrosome protein recruitment during the first cell cycle. The movement of centrosomes leading up to the first asymmetric division is highly regulated and controlled by the MT arrays they nucleate. Immediately after fertilization, the centrioles duplicate and initiate MT nucleation, which facilitate the migration of the maternal pronucleus. The pronuclei meet at the posterior end of the embryo and form the pronuclear complex (PNC). The PNC then migrates to the center of the embryo and rotates 90 degrees to align the centrosomes along the anterior-posterior axis, a process known as centration and rotation (C&R), which is crucial for establishing the orientation and position of the division plane for first division (Fig. 2a).

AIR-1, a protein homologous to Aurora Kinase A (AURKA), plays a key role in centrosome maturation by regulating the recruitment of pericentriolar material (PCM) proteins via protein phosphorylation. Depletion of AIR-1/AURKA in early *C. elegans* embryos via RNA interference results in malformed spindles and impaired centrosome maturation[21,22]. AIR-1/AURKA also acts to repress microtubule nucleation by activating KLP-7, a kinesin-like protein that inhibits microtubule nucleation at the centrosome[23]. Following a quantification and normalization protocol (Materials & Methods, Fig. 2b), we analyze time-lapse microscopy images of centrosomal GFP::AIR-1 fluorescence, allowing us to identify potential asymmetries in centrosomes during the critical positioning period, from pronuclear migration to nuclear envelope breakdown (NEBD). Our analysis reveals that both leading and lagging centrosomes undergo maturation by recruiting proteins such as AIR-1/AURKA, but lagging centrosomes exhibit higher average intensity of GFP::AIR-1 compared to the leaders (Fig. 2d). This observation is confirmed with statistical analysis by fitting a regression model with AR(1) within-subject correlation structure and indicator variable for the centrosome type (leading=0, lagging = 1) as detailed in Materials & Methods. The mean trajectories of the two centrosome types have similar slopes (Wald's test statistic for the difference in slopes is 1.09 with a p-value of 0.2973) but different intercepts, with the lagging centrosome's intercept significantly higher than the leader's intercept (Wald's test statistic for the difference in intercepts is 6.69 with p-value of 0.0097), indicating that the mean trajectory of the lagger is significantly above the mean trajectory of the leader. Additionally, while the cytoplasmic pool of GFP::AIR-1 decreases over this period, the total amount of GFP::AIR-1 slightly increases (Fig. 2c).

Centrosomal AIR-1 recovery

Centrosome maturation and asymmetric recruitment of AIR-1/AURKA discussed above occurs over a long timescale of approximately 330 s. To identify any asymmetries on a faster timescale, we use Fluorescence Recovery After Photobleaching (FRAP) shortly after pronuclear meeting (PNM), a time window not previously explored[24]. Using the *C. elegans* strain expressing GFP labeled AIR-1, we photobleached either the leading or lagging centrosome (10 of each) and tracked their recovery until AIR-1/AURKA levels stabilized, approximately 50 s (Fig. 3a). Individual time course data (Fig. 3b) was smoothed by fitting the exponential recovery model as detailed in the Methods. The computed recovery curve parameters indicate similar median values for the maximum recovery amount, V_{max} (1.5 for the leader and 1.4 for the lagger), and different median values for the half recovery time, $t_{1/2}$ (20.2 s for the leader and 15.7 s for the lagger). These values suggest a faster recovery for the lagger, potentially reflecting differences in the initial recovery dynamics (Fig. 3d). This observation is supported by mild statistical significance between the shapes of the average FRAP curves of leader versus lagger centrosomes during the initial period of recovery, assessed using a FRAP-specific statistical procedure.[25] As previously discussed,[25] testing for differences in specific parameters from fitted FRAP trajectories may be too restrictive to reveal differences in overall shapes of the recovery curves and may overlook biologically relevant differences. Instead, considering p-values from t-tests between means at each time point provides a more flexible method to detect differences in FRAP trajectory shapes. In our case, the p-values increase with time but show mild significance during the initial recovery stage (Fig. 3c), indicating a potential difference between the two centrosomes.

The model requires distinct centrosomes

To identify the specific dynamic factors underlying the observed asymmetry over extended time scales, we develop a comprehensive mathematical model of centrosome maturation that avoids bias from assumptions about centrosome identity. Our model consists of three compartments: two representing the centrosomes and a third representing the free supply of the model factor found in the cytoplasm (Fig. 4a). The model incorporates a dynamic cytoplasmic concentration, and centrosomes characterized by cooperativity, carrying capacity, and cytoplasmic flux (Eq. 6). Parameter sets were identified that best fit our *in vivo* AIR-1/AURKA data[26]. Model variants that assume the centrosomes have identical kinetics are not able to match the *in vivo* data as effectively as those model variants that treat centrosomes as distinct compartments (Extended Data Fig. 1), suggesting that the leader and lagger centrosomes have distinct AIR-1/AURKA recruitment dynamics.

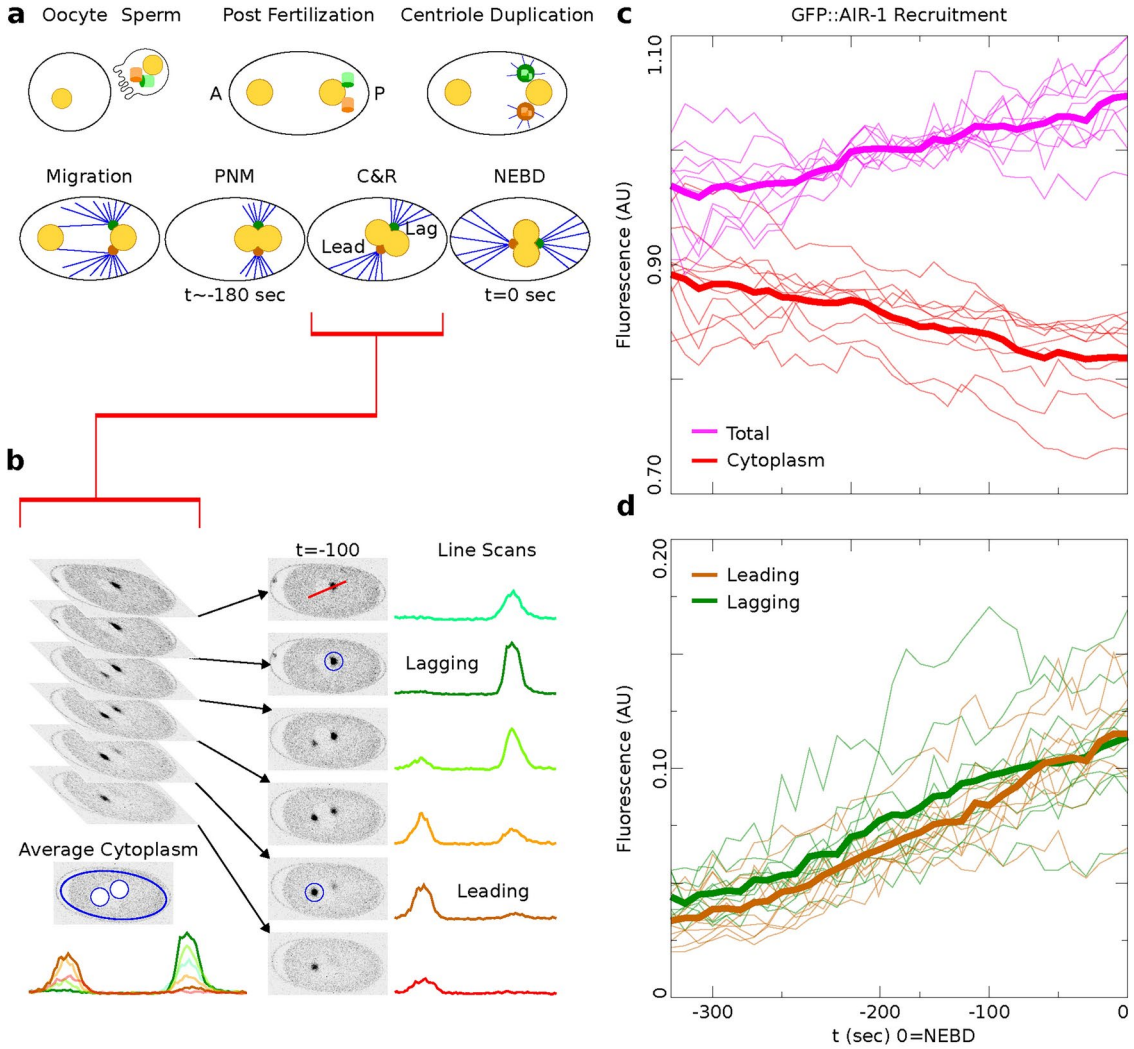

Figure 2. Recruitment of AIR-1/AURKA revealed by precise quantification of 4D microscopy. (**a**) *C. elegans* development steps leading up to the first division. The sperm donates the two centrioles and marks the posterior (P) of the embryo. Centrioles duplicate, and their centrosomes mature during migration, pronuclear meeting (PNM), centration and rotation (C&R), and nuclear envelope breakdown (NEBD). (**b**) Quantification of the centrosome using the brightest fluorescent signal. Line scans are used to visualize the fluorescence of the centrosomes; circles denote the measured area. (**c**,**d**) Individual time courses are plotted (thin lines) and averages (solid lines). (**c**) The cytoplasm (red) and the total (magenta). (**d**) The leading centrosome (orange) and the lagging centrosome (green) with mean lagger trajectory significantly higher than the mean leader trajectory (p-value for the difference is 0.0097 as detailed in Results).

The dynamics of the mathematical model

As the best fit to our model requires us to consider centrosomes as distinct compartments with their own dynamics, we construct three variants of the model representing different interactions to assess their impact on model fit. All three model variants produce comparable parameter distributions, yet the dynamic cytoplasm model consistently demonstrates a twofold reduction in fitting error to the *in vivo* data (Extended Data Fig. 1, Extended Data Fig. 2).

We continue our investigation with a mathematical model of centrosome dynamics by extending the dynamic cytoplasm model to include fluorescent (F) and bleached (B) versions of the model factor to simulate photobleaching (Eq. 1a–f, Fig. 4a). We identify 112 independent parameter sets that minimize error in simulations of recruitment (Fig. 4b) and recovery dynamics (Fig. 4c).

$$\frac{dC_{yb}}{dt} = -\alpha_7 C_{yb} - \frac{dC_{1b}}{dt} - \frac{dC_{2b}}{dt} \tag{1a}$$

$$\frac{dC_{yf}}{dt} = \frac{\alpha_6}{C_0 F} - \alpha_7 C_{yf} - \frac{dC_{1f}}{dt} - \frac{dC_{2f}}{dt} \tag{1b}$$

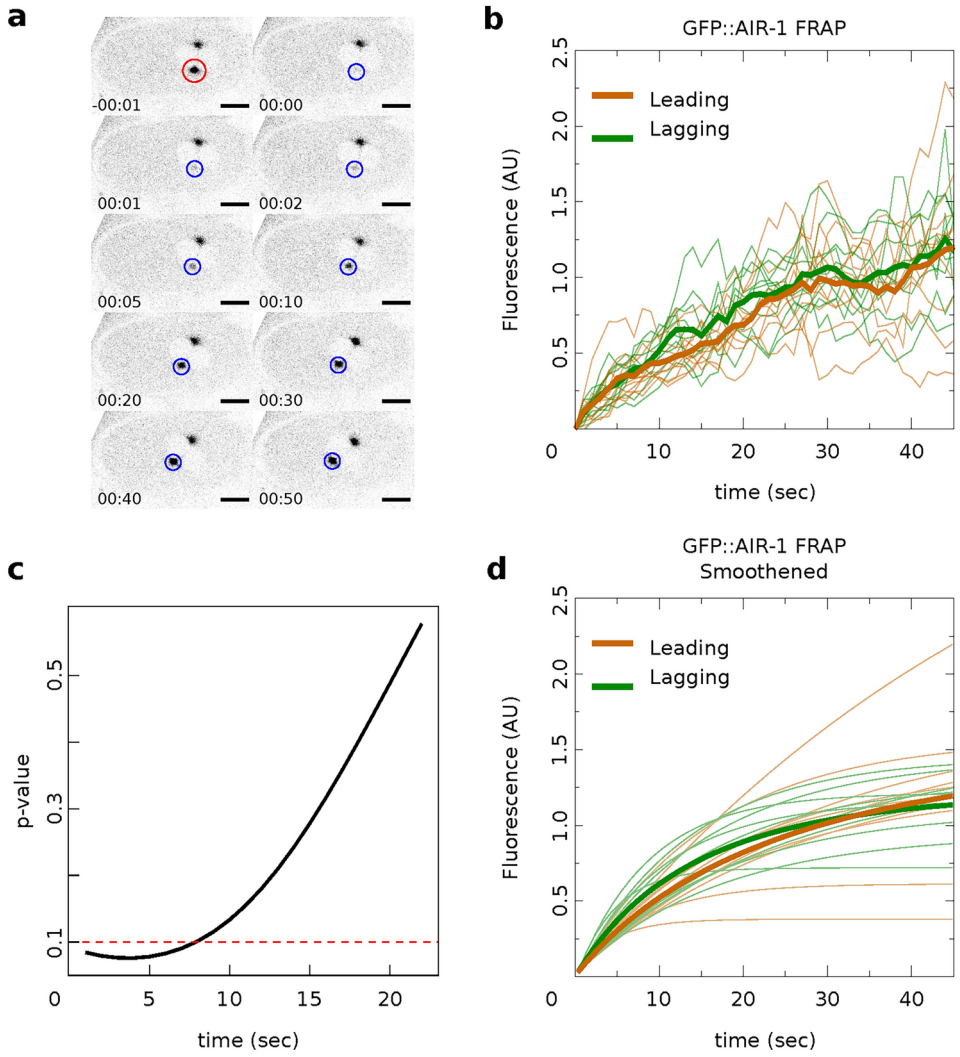

Figure 3. Recovery of AIR-1/AURKA observed on a short timescale using FRAP. (**a**) Example image of photobleaching of a single centrosome. Photobleaching was performed shortly after PNM and imaged every second for a total of 50 s (Scale bar: 10 μm). (**b**) Recovery curves (thin lines) and their averages (solid lines) for ten leading centrosomes (orange) and ten lagging centrosomes (green). Measurements were taken from 20 centrosomes (10 leader and 10 lagger) across 20 embryos. (**c**) p-values for FRAP-specific statistical procedure developed in[25]. Red line indicates significance level $\alpha = 0.1$. (**d**) Smoothed version of the data in (**b**) used to compute *p*-values in (**c**).

$$\frac{dC_{1b}}{dt} = C_0^{n1}\left(1 - \frac{C_{1b}B + C_{1f}F}{\alpha_4}\right) C_{yb}(C_{1b}B + C_{1f}F)^{n_1} - \alpha_1 C_{1b} \tag{1c}$$

$$\frac{dC_{1f}}{dt} = C_0^{n1}\left(1 - \frac{C_{1b}B + C_{1f}F}{\alpha_4}\right) C_{yf}(C_{1b}B + C_{1f}F)^{n_1} - \alpha_1 C_{1f} \tag{1d}$$

$$\frac{dC_{2b}}{dt} = \alpha_3 C_0^{n2}\left(1 - \frac{C_{2b}B + C_{2f}F}{\alpha_5}\right) C_{yb}(C_{2b}B + C_{2f}F)^{n_2} - \alpha_2 C_{2b} \tag{1e}$$

$$\frac{dC_{2f}}{dt} = \alpha_3 C_0^{n2}\left(1 - \frac{C_{2b}B + C_{2f}F}{\alpha_5}\right) C_{yf}(C_{2b}B + C_{2f}F)^{n_2} - \alpha_2 C_{2f} \tag{1f}$$

In the cytoplasmic compartment, the on rate (α_6) and off rate (α_7) exhibit a remarkably high linear correlation with an R^2 value of 0.9995 (Extended Data Fig. 4), indicating tightly regulated protein production and decay dynamics. By fitting these centrosome dynamics parameters to a 3D curve, we achieved precise estimation of cooperativity with minimal error relative to the other parameters of interest (Fig. 5a). Parameters governing the centrosome compartments, specifically cooperativity, inverse of the carrying capacity, and the ratio of the on rate to off rate, also show significant correlations (Fig. 5b). This suggests that the model parameters must be highly constrained in order to replicate dynamics that closely resemble the observed *in vivo* behavior. In particular,

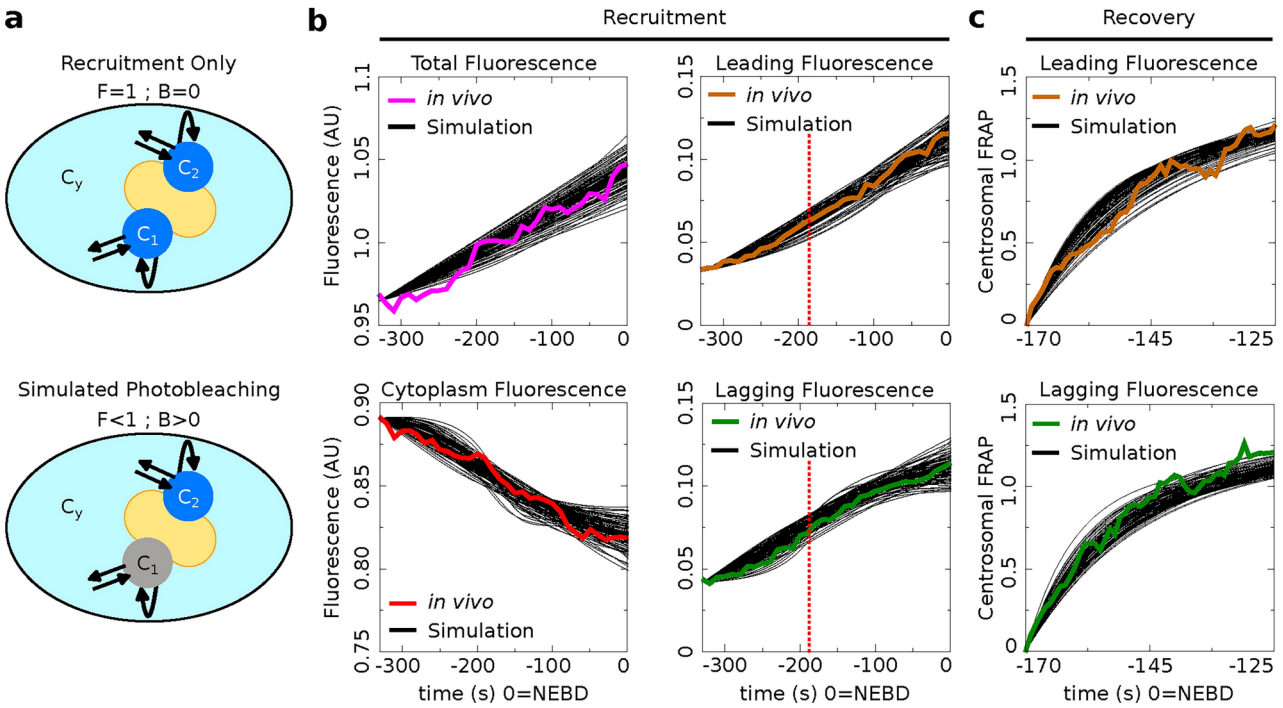

Figure 4. Simulations recapitulate the observed recruitment and recovery dynamics. (**a**) Schematic of our three-compartment centrosome maturation model and example of photobleaching compartment C_1. The model factor can transfer from the two centrosome compartments to the cytoplasm compartment as controlled by the model parameters. (**b–c**) Parameter sets produce simulated curves that match to (**b**) recruitment and (**c**) recovery. Red dotted lines indicate the time of PNM, when the FRAP analysis started.

we find that the leader and lagger centrosomes can inhabit distinct regions of the space defined by these three distinct features. The parameter space associated with the leading centrosome compartment appears to be a subset of that associated with the lagging compartment, suggesting that the leading centrosome predominantly exists in an older, lattice-like state, while the lagging centrosome is able to adopt a younger, condensate-like form[5] (Fig. 5c, Table 1).

Discussion

Understanding the structure and dynamics of maturing centrosomes is crucial for unraveling their role in cell fate decisions. To achieve this, we conducted targeted experiments examining the centriole and pericentriolar material (PCM), and developed a data validated mathematical model to elucidate the mechanisms underlying the distinct dynamics between the two centrosomes. Together, our results contribute to our understanding of the structural intricacies and the unique maturation dynamics of both centrosomes during early embryonic development.

We tracked centriole inheritance up to the four-cell stage to detect any potential bias in their distribution to the daughter cells. Our probability model indicates that the first division can yield either random or biased outcomes while still matching experimentally observed distributions, aligning with similar reports[20]. In various organisms, centriole maturation involves acquiring distal appendage proteins (DAPs), leading to structural and functional differences between mother and daughter centrioles[27,28], and age-related inheritance in specific cell types[13,14,17]. Unlike human cells, *C. elegans* centrioles are believed to lack orthologs of these DAPs. Instead, *C. elegans* centrosomes feature a unique structure known as the paddlewheel, which spans the entire length of mature centrioles[29,30]. Unlike DAPs, which are dispensable for division in human cells[30–33], paddlewheels are essential for proper cell division in *C. elegans*. However, the extent to which paddlewheel features affect centriole inheritance remains unclear.

To further investigate potential asymmetries in centrosome maturation, we quantified AIR-1/AURKA dynamics during this critical developmental process. We focused on the intensity of the GFP-AIR-1 signal rather than the size of the PCM because the boundaries of the centrosome are not well-defined. While centrosomes are thought to evolve from a dynamic, liquid-like state to a more solid, stable state with lower turnover[5], this change in centrosome state is not proposed to be associated with a change in the size of the centrosomes. To minimize potential confounding effects from centrosome growth and movement, we measured GFP fluorescence within a fixed area, using fluorescence intensity as a proxy for AIR-1/AURKA density in that region. The distinct long timescale recruitment and short timescale FRAP recovery dynamics of the leading and lagging centrosomes reveal that centrosomes are highly dynamic during maturation leading to the first division of the *C. elegans* embryo. The experimental data for both the recruitment and the recovery show differences between the leading

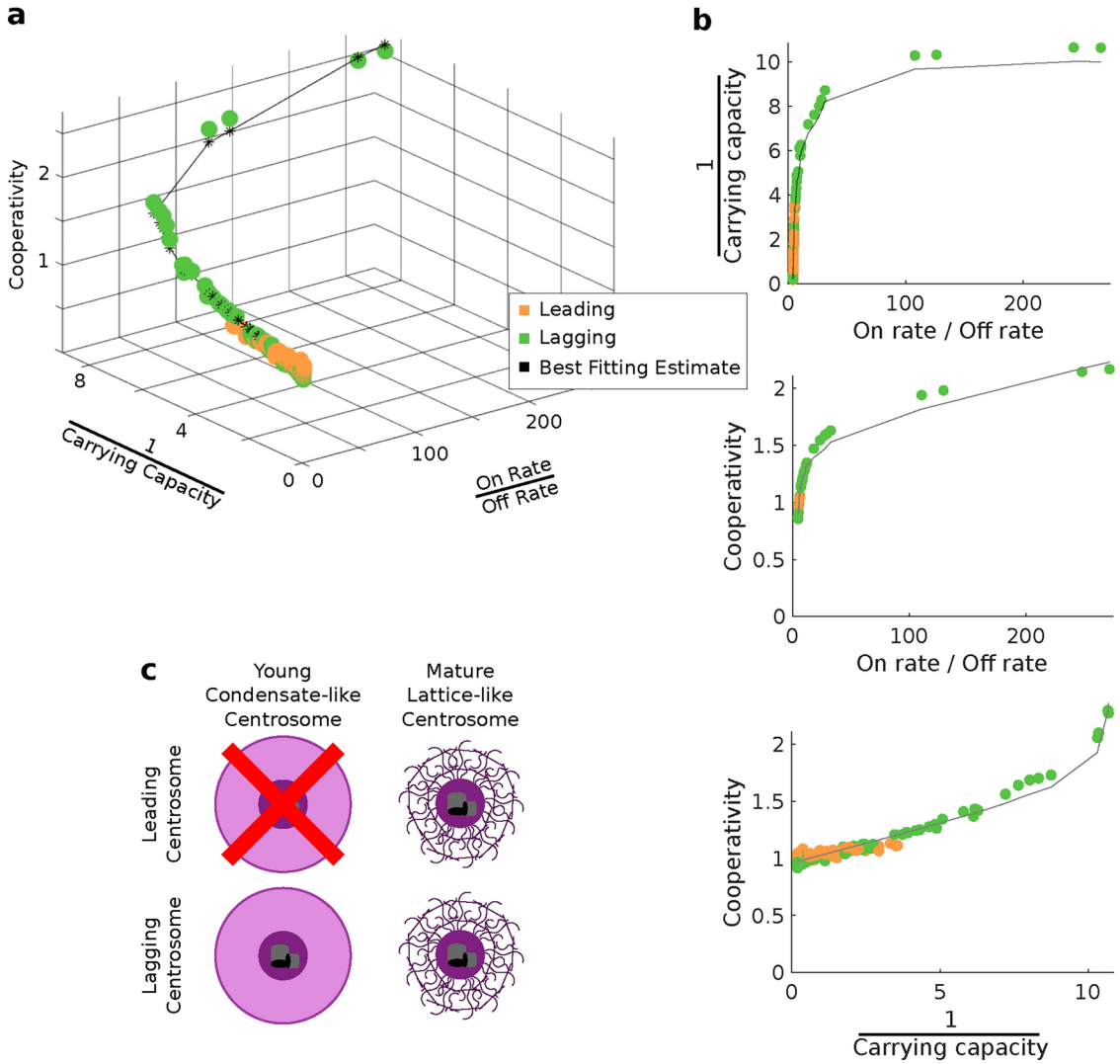

Figure 5. Parameter Analysis reveals tight regulation of simulated centrosome dynamics. (**a**) 3D plot and (**b**) of all parameter sets (on rate/off rate, 1/carrying capacity, cooperativity) fit to $z = 1.011 + 0.003x + 0.108y$ with an $R^2 = 0.971$ and RMSE of 0.040. Best fit estimates correspond to the calculated cooperativity values; see Extended Data Figure 6 for the full surface generated by the best-fit equation. (**c**) The four possible identities of the leading and lagging centrosome in terms of its centriole age. Our model indicates that the leading centrosome is not found in the younger and condensate-like state.

	Cooperativity	Turnover	$(\text{Carrying Capacity})^{-1}$
Leader	Low	Low	Low
Lagger	Low to High	Low to High	Low to High
Lattice	Low	Low	Low
Condensate	High	High	High

Table 1. Comparison of model features using the parameter sets that best fit the experimental data, with the characteristics of different types of centrosome structures as reported in previous studies.[5].

and the lagging centrosomes dynamics in both processes. These differences were highlighted by modeling results, where initially unbiased mathematical model fits the data significantly better when we accounting for different kinetics between the two centrosome compartments.

The parameters for our model analysis were identified through a comprehensive parameter search designed to explore a wide range of values with the only constraint being that the parameters are positive[34]. This approach ensures that the resulting parameter sets are not biased toward any specific range or relationships.

Our mathematical model reveals three distinct parameter regimes capable of producing dynamics consistent with the observed recruitment and recovery of centrosomal AIR-1/AURKA. The model demonstrates that within a single simulation, the two centrosomes can possess vastly different characteristics while still producing recruitment and recovery curves that align with our experimental data. In particular, the leading and lagging centrosomes have distinct dynamics, with the lagging centrosome having lower cooperativity in its AIR-1/AURKA recruitment dynamics compared to the leader. This is consistent with the lower density of microtubules in the lagging centrosome, possibly due to AIR-1/AURKA's activation of KLP-7, an inhibitor of microtubule nucleation at centrosomes[23]. In contrast, the leading centrosome exhibits higher cooperativity in its AIR-1/AURKA recruitment dynamics, resulting in lower levels of AIR-1/AURKA and KLP-7 during the early stages of centrosome maturation, promoting higher microtubule nucleation and highlighting the complex role of AIR-1/AURKA.

This study employs an interdiscplinary multiscale approach to investigate how structural variations at different scales affect centrosome characteristics. Our centriole inheritance data indicates that preferential centriole inheritance may occur while preserving observed centriole distributions at the four cell stage, and any differences in paternally derived centrioles could either be amplified or suppressed at the macroscale level of the centrosome's PCM. There are three prevailing biological models for centrosome structure: lattice, condensate, and transition, each supported by distinct experimental evidence[5]. Our combined use of multi-scale microscopy and mathematical modeling reveals distinct dynamic behaviors between the leading and lagging centrosomes (Table 1). Our analysis shows that the leading centrosome operates within a more restricted parameter space, indicating less dynamic behavior, while the lagging centrosome occupies a more dynamically variable state. This aligns with prior findings that centrosomes mature from a dynamic condensate-like state to a stable lattice-like state.

In future work, we will investigate whether asymmetries are present in other centrosome-associated proteins, including AIR-1/AURKA's upstream regulator SPD-5 and its downstream effectors TBG-1 and ZYG-9. SPD-5 plays a crucial role in assembling the pericentriolar material[35], while TBG-1 and ZYG-9 are involved in microtubule nucleation and stabilization.[36,37] Using similar analyses, we will determine whether the asymmetry observed with AIR-1/AURKA is unique or reflects a broader pattern of asymmetric recruitment at the centrosomes, providing additional insights into the mechanisms underlying asymmetries during centrosome maturation. We will further explore whether age-related differences or specific cues designate the paternally contributed mother and daughter centrioles as leading or lagging, and how this influences the centrosome's structure leading up to the first division of the *C. elegans* embryo. This study suggests that a more nuanced understanding of centrosome dynamics is necessary to fully understand cell fate determination and centrosome biology in *C. elegans* and other organisms.

Methods

Experimental methods

Nematode strains

The OD142 (ltIs78 [(pKO5) pie-1::GFP::TEV::Stag::air-1 spliced coding + unc-119(+)]), BA17 (fem-1(hc17) IV) strains were provided by the Caenorhabditis Genetics Center, which is funded by the National Institutes of Health (NIH) Office of Research Infrastructure Programs (P40 OD010440). The OD574 (unc-119(ed9)III; ltSi81[pY024; Psas-6::GFP::SAS-4 reencoded; cb-unc-119(+)]II) strain was a gift from Karen Oegema. Strains were maintained on nematode growth media agar plates seeded with OP50 Escherichia coli as a food source. Strain stocks were maintained at 20C by chunking or picking wild-type worms as needed and were stored at -80C according to standard practices.

Centriole tracking

Male OD574 GFP::SAS-4 worms were picked from starved plates to propagate. Feminized worms were generated from the BA17 strain by growing at 25C. Male OD574 organisms were picked to plates containing female BA17 worms and then, after mating overnight, were dissected and imaged as described below.

Fluorescence microscopy

Hermaphrodite worms were transferred to a coverslip with egg salts buffer (118 mM NaCl, 48 mM KCl, 2 mM MgCl2, 2 mM CaCl2, 0.025 mM HEPES, pH 7.4) and dissected to release embryos. Coverslips were then inverted onto slides with 2% agar pads (in egg salts buffer) and sealed with Petrolatum.

Centrosomal recruitment Time-lapse z-stacks were taken with 1.5 μm spacing, spanning 15 μm centered at the midplane of the embryo, with a 10s delay between stacks. Images were always collected from 100 s before PNM to second division to ensure the embryos divided with normal timing, indicating that they were healthy.

Centriole inheritance tracking z-stacks were taken with 1.0 μm spacing, spanning 7 μm centered at the mid-plane of the embryo. Images that did not capture two distinct centrioles were removed before analysis. 3 embryos had no identifiable GFP+ centrioles, and 4 only had one GFP+ centriole.

Image analysis

Image analysis and maximum-intensity projections shown in the figures were made in FIJI (Fiji Is Just ImageJ).

AIR-1 intensity plots Embryo images were rotated and flipped as necessary so that the anterior was at the left and the MTOC that went to the anterior started on the bottom. For each time point a single slice of the 10 slice z-stack was chosen to be analyzed, this slice represents the middle and brightest slice of the MTOC and we re-

quired 1 slice of the z-stack on both sides of it to ensure we were capturing the brightest slice possible. This was done independently for the leading and lagging MTOCs, and a new image sequence containing only these slices to be analyzed was generated.

Fluorescence recovery after photobleaching (FRAP)
Standard FRAP protocols were followed as previously described[24].

Recovery curve and fitting to an exponential Recovery parameters were calculated as follows:

$$V_{max}(1 - e^{-t/K_{off}}) \tag{1}$$

where V_{max} represents the Mobile Fraction of the fluorophore.

$$\tau_{1/2} = -ln(0.5)K_{off} \tag{2}$$

where $\tau_{1/2}$ represents the half time of recovery.

Theoretical methods

Normalization of data
The calculated fluorescence values with background removed were individually normalized by dividing each point by the average value of the total fluorescence, giving values that we can simulate in our model.

Error calculation
We defined the error between our simulated data and the AIR-1 fluorescence data as the point-wise sum of the differences between the two data sets.

$$\text{Error} = \sum_t |\text{Simulated Data(t)-Fluorescence Data(t)}| \tag{3}$$

Model selection
MTOC factor is capable of flowing from the cytoplasm to each of the compartments, k_{+1}, k_{+2} and back to the cytoplasm, k_{-1}, k_{-2}, where it is available for further patterning. The recruitment to each MTOC was limited by saturation, C_{1max}, C_{2max}, but promoted by the cooperativity of the compartment C_1^{n1}, C_2^{n2}. The following three models were implemented with different cytoplasmic dynamics to determine the best for our investigation.

To simulate the conservation of the MTOC factor, we used $C_y = C_0 - (C_1 + C_2)$ such that the amount of factor was equal to C_0 at all time points.

$$C_y = C_0 - (C_1 + C_2) \tag{4a}$$

$$\frac{dC_1}{dt} = k_{+1}\left(1 - \frac{[C_1]}{C_{1max}}\right)[C_y][C_1]^{n_1} - k_{-1}[C_1] \tag{4b}$$

$$\frac{dC_2}{dt} = k_{+2}\left(1 - \frac{[C_2]}{C_{2max}}\right)[C_y][C_2]^{n_2} - k_{-2}[C_2] \tag{4c}$$

When we simulate a quasi-steady state we use $C_y = C_0$ such that the amount of factor in the cytoplasm is equal to C_0 at all time points.

$$C_y = C_{y0} \tag{5a}$$

$$\frac{dC_1}{dt} = k_{+1}\left(1 - \frac{[C_1]}{C_{1max}}\right)[C_y][C_1]^{n_1} - k_{-1}[C_1] \tag{5b}$$

$$\frac{dC_2}{dt} = k_{+2}\left(1 - \frac{[C_2]}{C_{2max}}\right)[C_y][C_2]^{n_2} - k_{-2}[C_2] \tag{5c}$$

The cytoplasm can gain and lose model factor k_{+3}, k_{-3}

$$\frac{dC_y}{dt} = k_{+3} - k_{-3}[C_y] - \frac{dC_1}{dt} - \frac{dC_2}{dt} \tag{6a}$$

$$\frac{dC_1}{dt} = k_{+1}\left(1 - \frac{[C_1]}{C_{1max}}\right)[C_y][C_1]^{n_1} - k_{-1}[C_1] \tag{6b}$$

$$\frac{dC_2}{dt} = k_{+2}\left(1 - \frac{[C_2]}{C_{2max}}\right)[C_y][C_2]^{n_2} - k_{-2}[C_2] \tag{6c}$$

As described in the results, the Dynamic cytoplasm had a two fold better fit by our error metric and the parameter sets were all consistent between the three models (Extended Data Fig. 1, Extended Data Fig. 2).

Mathematical model

With the dynamic cytoplasm model chosen, we then wanted to simulate the photobleaching of the MTOCs. This required constructing a set of equations for two separate populations of model factor, a fluorescent population and a bleached population. We included a bleached factor and a fluorescent factor to account for the simulated photobleaching. We required this model to account for the photobleaching without changing the dynamics of the original model. The sum of bleached factor (C_b) and fluorescent factor (C_f) would behave exactly as in a model with just a fluorescent factor. These features are incorporated into a set of differential equations describing the change in concentration of the MTOC factor in each compartment over time, resulting in Eq. 7. We converted these equations into their dimensionless forms, as the specific parameter values for these generic MTOC factors cannot be directly estimated, resulting in Eq. 1.

$$\frac{C_{yb}}{dt} = -k_{-3}C_{yb} - \frac{dC_{1b}}{dt} - \frac{dC_{2b}}{dt} \tag{7a}$$

$$\frac{C_{yf}}{dt} = k_{+3} - k_{-3}[C_{yf}] - \frac{dC_1}{dt} - \frac{dC_2}{dt} \tag{7b}$$

$$\frac{dC_{1b}}{dt} = k_{+1}\left(1 - \frac{[C_{1b}] + [C_{1f}]}{C_{1max}}\right)[C_{yb}]([C_{1b}] + [C_{1f}])^{n_1} - k_{-1}[C_{1b}] \tag{7c}$$

$$\frac{dC_{1f}}{dt} = k_{+1}\left(1 - \frac{[C_{1b}] + [C_{1f}]}{C_{1max}}\right)[C_{yf}]([C_{1b}] + [C_{1f}])^{n_1} - k_{-1}[C_{1f}] \tag{7d}$$

$$\frac{dC_{2b}}{dt} = k_{+2}\left(1 - \frac{[C_{2b}] + [C_{2f}]}{C_{2max}}\right)[C_{yb}]([C_{2b}] + [C_{2f}])^{n_2} - k_{-2}[C_{2b}] \tag{7e}$$

$$\frac{dC_{2f}}{dt} = k_{+2}\left(1 - \frac{[C_{2b}] + [C_{2f}]}{C_{2max}}\right)[C_{yf}]([C_{2b}] + [C_{2f}])^{n_2} - k_{-2}[C_{2f}] \tag{7f}$$

At any specified time, we can simulate photobleaching in the model by transferring all, or a proportion, of the fluorescent model factor to the bleached factor in a compartment.

$$\frac{dC_y^*}{dt^*} = \frac{\alpha_6}{C_0} - \alpha_7 C_y^* - \frac{dC_1}{dt} - \frac{dC_2}{dt} \tag{8a}$$

$$\frac{dC_1^*}{dt^*} = C_0^{n_1}\left(1 - \frac{C_1^*}{\alpha_4}\right)C_y^*(C_1^*)^{n_1} - \alpha_1 C_1^* \tag{8b}$$

$$\frac{dC_2^*}{dt^*} = \alpha_3 C_0^{n_2}\left(1 - \frac{C_2^*}{\alpha_5}\right)C_y^*(C_2^*)^{n_2} - \alpha_2 C_2^* \tag{8c}$$

$$\frac{dC_{yb}^*}{dt^*} = -\alpha_7 C_{yb}^* - \frac{dC_{1b}^*}{dt^*} - \frac{dC_{2b}^*}{dt^*} \tag{9a}$$

$$\frac{dC_{yf}^*}{dt^*} = \frac{\alpha_6}{C_0 F} - \alpha_7 C_{yf}^* - \frac{dC_{1f}^*}{dt^*} - \frac{dC_{2f}^*}{dt^*} \tag{9b}$$

$$\frac{dC_{1b}^*}{dt^*} = C_0^{n1}\left(1 - \frac{C_{1b}^* B + C_{1f}^* F}{\alpha_4}\right)C_{yb}^*(C_{1b}^* B + C_{1f}^* F)^{n_1} - \alpha_1 C_{1b}^* \tag{9c}$$

$$\frac{dC_{1f}^*}{dt^*} = C_0^{n1}\left(1 - \frac{C_{1b}^* B + C_{1f}^* F}{\alpha_4}\right)C_{yf}^*(C_{1b}^* B + C_{1f}^* F)^{n_1} - \alpha_1 C_{1f}^* \tag{9d}$$

$$\frac{dC_{2b}^*}{dt^*} = \alpha_2 C_0^{n2}\left(1 - \frac{C_{2b}^* B + C_{2f}^* F}{\alpha_5}\right)C_{yb}^*(C_{2b}^* B + C_{2f}^* F)^{n_2} - \alpha_3 C_{2b}^* \tag{9e}$$

$$\frac{dC_{2f}^*}{dt^*} = \alpha_2 C_0^{n2}\left(1 - \frac{C_{2b}^* B + C_{2f}^* F}{\alpha_5}\right)C_{yf}^*(C_{2b}^* B + C_{2f}^* F)^{n_2} - \alpha_3 C_{2f}^* \tag{9f}$$

Modified metropolis hastings

The modified Metropolis-Hastings (MMH) algorithm is an iterative algorithm with the goal of minimizing some measurable quantity. Starting from an initial random parameter set as the seed, the MMH algorithm randomly generates a new parameter set where each parameter is selected from a normal distribution centered on the seed's value with a standard deviation we set to be 90% of that value. The total error from the simulated fluorescence data to the actual fluorescence of AIR-1 was calculated and compared to the error calculated from

the seed parameter set. If the new parameter set had a lower error it was selected as the seed for future iterations, if the error was higher it was discarded and the previous seed remained. This process was repeated until the error satisfied our end condition giving us a single parameter set that produced simulated data matching our AIR-1 fluorescence.

Inheritance analysis

Given the distribution of the fluorescent centrioles follows a series of independent Bernoulli trials, the probability of each possible fluorescence profile can be written as in Eq. 10.

$$P_{P_2}^{ABa} = \lambda_1\lambda_2\lambda_3 + (1-\lambda_1)\lambda_4\lambda_5 \tag{10a}$$

$$P_{EMS}^{ABa} = \lambda_1(1-\lambda_2)\lambda_3 + (1-\lambda_1)(1-\lambda_4)\lambda_5 \tag{10b}$$

$$P_{P_2}^{ABp} = \lambda_1\lambda_2(1-\lambda_3) + (1-\lambda_1)\lambda_4(1-\lambda_5) \tag{10c}$$

$$P_{EMS}^{ABp} = \lambda_1(1-\lambda_2)(1-\lambda_3) + (1-\lambda_1)(1-\lambda_4)(1-\lambda_5) \tag{10d}$$

Statistical analysis

The standard statistical tests performed in this paper (paired T-test, Pearson correlation, Kolmogorov-Smirnov test) were implemented in Matlab or R using standard built-in functions.

Two additional methods were implemented for analysis of the AIR-1 recruitment (Fig. 2) and recovery (Fig. 3). For the recruitment data, we fit the linear model

$$\mathbb{E}(\text{flourescence}|\text{time}) = \beta_0 + \beta_1 \cdot \text{time} + \beta_2 \cdot \text{type} + \beta_3 \cdot \text{time*type}$$

where the "type" is the indicator variable which equals to 0 if type = leading and equals to 1 if type = lagging (see, e.g., Sect. 5.1 of[38] for the description of this type of models). We used the AR(1) correlation structure to account for correlations between observations that belong to the same embryo (see, e.g., Sect. 7.3 of[38] for correlation structures in models of this type). Coefficient estimation and testing was performed using the R package *geepack*[39].

For the recovery data, we smoothed the raw trajectories by fitting the exponential recovery model as detailed in Sect. 4.2 (Fig. 3d). Adopting the FRAP-specific methodology developed in[25], we performed pairwise t-testing between mean trajectories for each time point and reported the p-value over time (Fig. 3c).

Data availability

Our data and code are available in the following public GitHub repository. https://github.com/Shayne-Falco/CentrosomeStructure_ModelsData.

Received: 24 July 2024; Accepted: 13 January 2025
Published online: 13 March 2025

References

1. Robbins, E., Jentzsch, G. & Micali, A. The centriole cycle in synchronized HeLa cells. *J. Cell Biol.* **36**(2), 329–339 (1968).
2. Vertii, A., Hehnly, H. & Doxsey, S. The centrosome, a multitalented renaissance organelle. *Cold Spring Harbor Perspect. Biol.***8**(12) (2016).
3. Godinho, S. A. & Pellman, D. Causes and consequences of centrosome abnormalities in cancer. *Philos. Trans. R. Soc. B: Biol. Sci.* **369**(1650), 9 (2014).
4. Coffman, V. C., McDermott, M. B. A., Shtylla, B. & Dawes, A. T. Stronger net posterior cortical forces and asymmetric microtubule arrays produce simultaneous centration and rotation of the pronuclear complex in the early Caenorhabditis elegans embryo. *Mol. Biol. Cell* **27**(22), 3550–3562 (2016).
5. Woodruff, J. B. The material state of centrosomes: lattice, liquid, or gel?. *Curr. Opin. Struct. Biol.* **66**, 139–147 (2021).
6. Delattre, M. et al. Centriolar SAS-5 is required for centrosome duplication in *C. elegans*. *Nat. Cell Biol.* **6**(7), 656–664 (2004).
7. Palazzo, R. E., Vogel, J. M., Schnackenberg, B. J., Hull, D. R. & Xingyong, W. Centrosome maturation. *Curr. Top. Dev. Biol.* **49**, 449–470 (1999).
8. Gönczy, P., Pichler, S., Kirkham, M. & Hyman, A. A. Cytoplasmic dynein is required for distinct aspects of MTOC positioning, including centrosome separation, in the one cell stage Caenorhabditis elegans embryo. *J. Cell Biol.* **147**(1), 135–150 (1999).
9. Kimura, A. & Onami, S. Computer simulations and image processing reveal length-dependent pulling force as the primary mechanism for C elegans male pronuclear migration. *Dev. Cell* **8**(5), 765–775 (2005).
10. Kimura, A. & Onami, S. Local cortical pulling-force repression switches centrosomal centration and posterior displacement in C elegans. *J. Cell Biol.* **179**(7), 1347–1354 (2007).
11. Kimura, K. & Kimura, A. Intracellular organelles mediate cytoplasmic pulling force for centrosome centration in the Caenorhabditis elegans early embryo. *Proc. Natl. Acad. Sci. USA* **108**(1), 137–142 (2011).
12. Shinar, T., Mana, M., Piano, F. & Shelley, M. J. A model of cytoplasmically driven microtubule-based motion in the single-celled Caenorhabditis elegans embryo. *Proc. Natl. Acad. Sci. USA* **108**(26), 10508–10513 (2011).
13. Macara, I. G. & Mili, S. Polarity and differential inheritance-universal attributes of life?. *Cell* **135**, 801–812 (2008).
14. Yamashita, Y. M. Regulation of asymmetric stem cell division: Spindle orientation and the centrosome. *Front. Biosci.* **14**, 3003 (2009).
15. Yamashita, Y. M., Mahowald, A. P., Perlin, J. R. & Fuller, M. T. Asymmetric inheritance of mother versus daughter centrosome in stem cell division. *Science* **315**(5811), 518–521 (2007).
16. Pelletier, L. & Yamashita, Y. M. Centrosome asymmetry and inheritance during animal development. *Curr. Opin. Cell Biol.* **24**(4), 541–546 (2012).
17. Wang, X. et al. Asymmetric centrosome inheritance maintains neural progenitors in the neocortex. *Nature* **461**(7266), 947–955 (2009).

18. Jankele, R., Jelier, R. & Gönczy, P. Physically asymmetric division of the *C. elegans* zygote ensures invariably successful embryogenesis. *eLife* **10**, 1–66 (2021).
19. Balestra, F. R., Von Tobel, L. & Gönczy, P. Paternally contributed centrioles exhibit exceptional persistence in *C. elegans* embryos. *Cell Res.* **25**(5), 642–644 (2015).
20. Gönczy, P. & Balestra, F. R. Sperm-contributed centrioles segregate stochastically into blastomeres of 4-cell stage Caenorhabditis elegans embryos. *Genetics* **224**(1), 48 (2023).
21. Toya, M., Terasawa, M., Nagata, K., Iida, Y. & Sugimoto, A. A kinase-independent role for Aurora A in the assembly of mitotic spindle microtubules in Caenorhabditis elegans embryos. *Nature Cell Biol.* **13**(6), 708–715 (2011).
22. Eva, H., Matthew, K., Anthony Hyman, A. & Oegema, K. Aurora-A kinase is required for centrosome maturation in Caenorhabditis elegans. *J. Cell Biol.* **155**(7), 1109–1115 (2001).
23. Han, X., Adames, K., Sykes, E. M. E. & Srayko, M. The KLP-7 residue S546 is a putative Aurora kinase site required for microtubule regulation at the centrosome in *C. elegans*. *PLoS ONE* **10**(7), e0132593 (2015).
24. Kress, E. et al. The UBXN-2/p37/p47 adaptors of CDC-48/p97 regulate mitosis by limiting the centrosomal recruitment of Aurora A. *J. Cell Biol.* **201**(4), 559–575 (2013).
25. Medina-Ruíz, G. I., Medina-Ruiz, A. I. & Morán, J. Fraping: A computational tool for detecting slight differences in fluorescence recovery after photobleaching (FRAP) data for actin polymerization analysis. *Microsc. Res. Tech.* **87**(7), 1541–1551 (2024).
26. Kravtsova, N., Chamberlin, H. M. & Dawes, A. T. Efficient parameter generation for constrained models using MCMC. *Sci. Rep.* **13**(1), 16285 (2023).
27. Ma, D., Wang, F., Teng, J., Huang, N. & Chen, J. Structure and function of distal and subdistal appendages of the mother centriole. *J. Cell Sci.* **136**(3), 2 (2023).
28. Tanos, B. E. et al. Centriole distal appendages promote membrane docking, leading to cilia initiation. *Genes Dev.* **27**(2), 163–168 (2013).
29. Woglar, A. et al. Molecular architecture of the *C. elegans* centriole. *PLoS Biol.* **20**(9), e3001784 (2022).
30. Sugioka, K. et al. Centriolar SAS-7 acts upstream of SPD-2 to regulate centriole assembly and pericentriolar material formation. *eLife* **6**, 1 (2017).
31. Paintrand, M., Moudjou, M., Delacroix, H. & Bornens, M. Centrosome organization and centriole architecture: Their sensitivity to divalent cations. *J. Struct. Biol.* **108**(2), 107–128 (1992).
32. Vorobjev, I. A. & Chentsov, Yu. S. Centrioles in the cell cycle I Epithelial cells. *J. Cell Biol.* **93**(3), 938–949 (1982).
33. Ishikawa, H., Kubo, A., Tsukita, S. & Tsukita, S. Odf2-deficient mother centrioles lack distal/subdistal appendages and the ability to generate primary cilia. *Nature Cell Biol.* **7**(5), 517–524 (2005).
34. Kravtsova, N., McGee, R. L. & Dawes, A. T. Scalable Gromov–Wasserstein based comparison of biological time series. *Bull. Math. Biol.* **85**(8), 8 (2023).
35. Nakajo, M., Kano, H., Tsuyama, K., Haruta, N. & Sugimoto, A. Centrosome maturation requires phosphorylation-mediated sequential domain interactions of SPD-5. *J. Cell Sci.* **135**(8), jcs259025 (2022).
36. Tabish, M. Expression of gamma-tubulin during the development of nematode Caenorhabditis elegans. *Mol. Biol. Rep.* **34**(4), 233–240 (2007).
37. Srayko, M., Quintin, S., Schwager, A. & Hyman, A. A. Caenorhabditis elegans TAC-1 and ZYG-9 form a complex that is essential for long astral and spindle microtubules. *Curr. Biol.* **13**(17), 1506–1511 (2003).
38. Weisberg, S. *Applied Linear Regression*. Wiley (2005).
39. Højsgaard, S., Halekoh, U. & Yan, J. The R package geepack for generalized estimating equations. *J. Stat. Softw.* **15**, 1–11 (2006).

Acknowledgements

Some strains were provided by the CGC, which is funded by NIH Office of Research Infrastructure Programs (P40 OD010440). This work is supported by NIH grant R01GM132651 to A.T.D.

Author contributions

S.M.P. contributed conceptualization, methodology, formal analysis, coding, investigation, visualization, writing-original draft, writing-review and editing. N.K. contributed Methodology and formal analysis. A.T.D. contributed conceptualization, methodology, formal analysis, investigation, writing-original draft, writing-review and editing, and supervision.

Declarations

Competing interests

All other authors declare no competing interests.

Additional information

Supplementary Information The online version contains supplementary material available at https://doi.org/10.1038/s41598-025-86548-0.

Correspondence and requests for materials should be addressed to A.T.D.

Reprints and permissions information is available at www.nature.com/reprints.

Publisher's note Springer Nature remains neutral with regard to jurisdictional claims in published maps and institutional affiliations.